Agrociencia

DYNAMIC CHARACTERISTICS OF MEMBRANE-TYPE AIR SPRINGS WITH AUXILIARY CHAMBER

Chunyan **Kong***, Xiaotong **Liu,** Xian **Wang,** Shunyao **Wang,** Guangli **Liu,** Mingkun **Yang,** Shuangshuang **Li**

Xihua University. School of Mechanical Engineering. Chengdu 610039, China.
* Author for correspondence: kongcy@mail.xhu.edu.cn

Citation: Kong C, Liu X, Wang X, Wang S, Liu G, Yang M, Li S. 2026. Dynamic characteristics of membrane-type air springs with auxiliary chamber. **Agrociencia.** https://doi.org/ 10.47163/agrociencia.v60i2.3579

Editor in Chief:
Dr. Fernando C. Gómez Merino

Received: November 19, 2025.
Approved: March 10, 2026.
Published in Agrociencia: March 24, 2026.

ABSTRACT

Air springs with auxiliary chambers are widely used by automobile manufacturers due to their lightweight design, low noise, superior shock absorption performance, and adjustable stiffness. The structural parameters of the auxiliary chamber and connecting pipeline play a decisive role in the shock absorption performance of air springs. This paper established a numerical simulation model for air springs with auxiliary chambers and studied the influence of the connecting pipeline diameter and the auxiliary chamber volume on the dynamic characteristics of air springs. The results indicate that, under the same initial internal pressure, the position where the stiffness tends to flatten shifts to higher frequencies as the pipeline diameter increases. As the pipeline diameter increased, the auxiliary chamber affected the stiffness over a broader frequency range. At lower loading frequencies, smaller pipeline diameters had a greater impact on stiffness, while larger pipeline diameters had a lesser impact. As the frequency increases, larger pipeline diameters gradually exert a stronger influence on stiffness. Between 2 and 6 Hz, the stiffness under different initial internal pressures decreased as the auxiliary chamber volume increased, while between 14 and 30 Hz, the opposite trend was observed. At all loading frequencies, the stiffness under different initial internal pressures decreased with increasing auxiliary chamber volume at 2 Hz, but as the loading frequency increased, this trend gradually reversed.

Keywords: Agricultural engineering, agricultural machinery, numerical simulation, stiffness, connecting pipe, finite element analysis.

INTRODUCTION

At present, the springs used in vehicles are mainly divided into two categories: ordinary springs and air springs (Figure 1). Ordinary springs include leaf springs, helical springs, and torsion bar springs. As modern automotive design and manufacturing have become increasingly aware of the importance of passenger comfort, air springs are increasingly being adopted by automakers due to their lightweight design, low noise, superior shock absorption performance, and road friendliness. Based on different structures of their air bags, air springs can be classified into three types: membrane-type, bellows-type, and sleeve-type (Kong *et al.*, 2025).

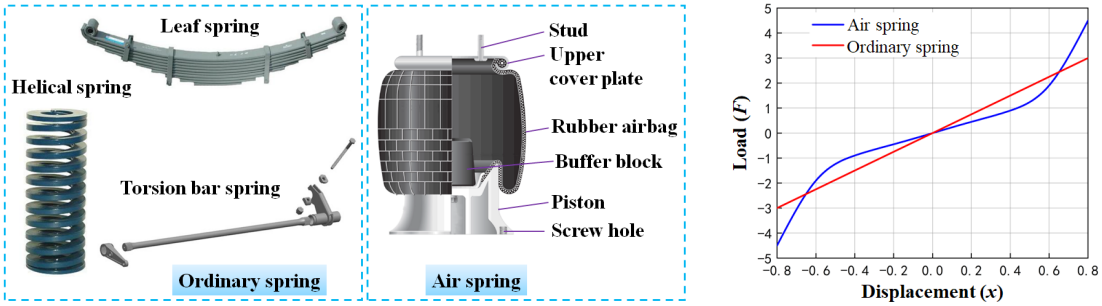

Figure 1. Comparison of springs used in vehicles.

Membrane-type air springs are commonly utilized in passenger vehicles due to their lower stiffness compared to bellows-type air springs. They also possess a straightforward structure, which allows for variations in elastic characteristics by simply adjusting structural parameters (Atindana *et al.*, 2023; Van and Tung, 2023). However, traditional single-chamber air springs are now struggling to meet people's demands for vehicle ride smoothness. Therefore, this paper focused on the study of membrane-type air springs with auxiliary chambers (ASWAC). Due to the influence of connecting pipelines and auxiliary chambers, the stiffness characteristics of ASWAC differ significantly from those of single-chamber air springs. The structural parameters of the connecting pipeline and auxiliary chamber present major challenges in ASWAC research (Zheng *et al*., 2016).

Numerous scholars, both domestically and internationally, have investigated this topic. Toyofuku *et al*. (1999) proposed a model to analyze the dynamic characteristics of air springs equipped with auxiliary chambers and pipelines, considering the relationship between vibration frequency and spring response and examining the effect of the pipeline on the dynamic spring constant. Zhang *et al*. (2020) verified the effectiveness of a proposed semi-active control system for air suspensions through numerical simulations. Mendia-García *et al*. (2022) used the Abaqus software to analyze the effects of selected structural parameters and initial internal pressure on the load-bearing performance of the main air chamber. These studies offer limited information on the structural parameters of ASWAC. As a result, it is challenging to accurately characterize the relationships and variation patterns between the structural parameters of the connecting pipelines and auxiliary chambers, as well as their dynamic stiffness.

This paper takes the air spring of a certain Mercedes-Benz model as the structural basis and adds an auxiliary chamber to it (Figure 2). By utilizing the Fluent software, a finite element simulation model is established to explore the variation patterns between the auxiliary chamber and its connecting pipeline and the dynamic characteristics of the air spring. This provides a certain theoretical foundation for the design and development of membrane-type ASWAC.

Figure 2. Structural configuration of the modified air suspension assembly.

MATERIALS AND METHODS

Theoretical basis of air springs with auxiliary chambers

The physical model of the air spring system with an auxiliary chamber (Figure 3) consists of a main chamber that includes a rubber bladder, an upper cover plate, and a piston. The auxiliary chamber comprises a cavity, and the main chamber is connected to the auxiliary chamber through a pipeline (Piller *et al*., 2002). Wherein P_1, V_1, and T_1 represent the absolute pressure, gas volume, and gas temperature in the main chamber, respectively; P_2, V_2, and T_2 represent the absolute pressure, gas volume, and gas temperature in the auxiliary chamber, respectively; and P_g, V_g, and T_g represent

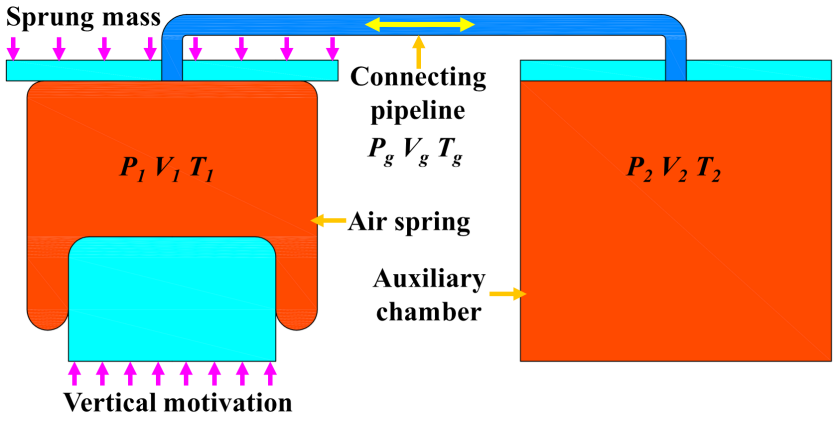

Figure 3. Physical model of the air spring system with auxiliary chamber and connecting pipeline.

the absolute pressure, gas volume, and gas temperature in the pipeline, respectively. During the operation of an air spring, its primary load comes from forces acting in the vertical direction (Chen *et al*., 2011; Wong *et al*., 2024). In this study, only the vertical motion of the air spring was considered.

While a vehicle is driving on the road, it experiences vibrations due to road irregularities or other external excitations. These vibrations are transmitted to the air spring through the vehicle's suspension system, causing deformation of the bladder in the main chamber. As the excitation intensifies, the air spring undergoes significant up-and-down vibrations, which alter its internal volume and pressure. At this point, changes in the internal pressure of the bladder will cause gas to flow between the main chamber and the auxiliary chamber, which are connected by a pipeline or orifice. The auxiliary chamber, serving as an additional volume, can accommodate more gas, thereby buffering the changes in pressure within the main chamber to a certain extent. The orifice or pipeline plays a crucial role in the process of gas flow (Karpenko *et al*., 2023; Mehmood *et al*., 2023). They not only restrict the gas flow velocity but also create a certain damping effect during the flow. This damping effect helps to attenuate vibrations, enabling the air spring to better absorb and disperse impacts from the road surface (Karachinskii and Timofeev, 2023). Through the synergistic effect of the main chamber, auxiliary chamber, and orifice or pipeline, the ASWAC can maintain stable performance under different vibration conditions.

The energy conservation equation for the main chamber of an ASWAC was defined as follows (Wissink, 2003; Zhang *et al*., 2005; Zhu *et al*., 2008):

$$dQ_1 + d(h_{1in} - h_{1out}) + dW_1 = dE_1$$

where Q_1 represents the heat exchange between the main chamber of the air spring and the external environment; h_{1in} is the inflow enthalpy of the main chamber; h_{1out} is the outflow enthalpy of the main chamber; W_1 is the work done by external forces on the main chamber; and E_1 is the total energy of the gas within the main chamber.

Similarly, based on the energy conservation equation for the main chamber, the energy conservation equation for the auxiliary chamber can be expressed as:

$$dQ_2 + d(h_{2in} - h_{2out}) + dW_2 = dE_2$$

where Q_2 represents the heat exchange between the auxiliary chamber of the air spring and the external environment; h_{2in} is the inflow enthalpy of the auxiliary chamber; h_{2out} is the outflow enthalpy of the auxiliary chamber; W_2 is the work done by external forces on the auxiliary chamber; and E_2 is the total energy of the gas within the auxiliary chamber.

When an ASWAC is in operation, due to the presence of the connecting pipeline, an exchange of gas and energy occurs between the main chamber and the auxiliary

chamber (Berg, 2000; Quaglia and Sorli, 2001). Therefore, the energy conservation equation and the gas state equation were used to describe the process of air changes within the air spring and the auxiliary reservoir. The gas flow rate equation was utilized to describe the mass exchange of air between the air spring and the auxiliary reservoir. To simplify the problem, discussions were held regarding the following scenarios:

1) During the operation of an air spring, as the frequency of displacement excitation increases, heat exchange between the air spring and the auxiliary chamber with the external environment becomes extremely difficult. When the amplitude of displacement excitation in the main chamber of the air spring is limited to ±10 mm, the gas exchange between the main and auxiliary chambers decreases (Williams, 1997; Mao *et al*., 2023).
2) In general, the air spring and the auxiliary chamber are installed in a basically horizontal position on a vehicle, with almost zero height difference between them. Therefore, the potential and kinetic energy between the main chamber of the air spring and the auxiliary chamber can be ignored.
3) According to the static experimental results of automotive air springs (Liu and Lee, 2011), when the excitation amplitude is ±10 mm, the relative error in the effective area change is only 6.37 %. Therefore, when conducting theoretical modeling, the effective area can be treated as a constant.

Establishment of a finite element model

According to Kong *et al*. (2024), the characteristics of the main chamber of the air spring under different initial internal pressures and displacements were analyzed. The loads and actual internal pressures of the main chamber under these conditions were obtained. Therefore, the equivalent area of the air spring at different initial internal pressures and displacements could be calculated (Table 1).

The equivalent area of the air spring within an excitation amplitude of ±10 mm was calculated under different initial internal pressures (Figure 4). At the same initial internal pressure, the equivalent area of the air spring varies slightly within a certain range for different displacements. The maximum difference in area occurs at an initial pressure of 0.25 MPa, with a value of 693.0939 mm², which is relatively small. Furthermore, taking the equivalent area at a displacement of 0 mm as the reference value, it can be determined that the maximum relative error in the equivalent area of the air spring appears at an initial internal pressure of 0.2 MPa, and it is only 2.45 %. Therefore, in this simulation experiment, when the excitation amplitude is ±10 mm, the effective area of the air spring can be considered a constant value.

The overall structure of the ASWAC is relatively simple, consisting solely of the main air chamber, connecting pipeline, and auxiliary chamber. By simplifying this structure and only considering the internal flow field, the finite element model was obtained (Figure 5).

Table 1. Equivalent effective area of the air spring within ±10 mm displacement under varying initial internal pressures (0.1–0.3 MPa).

Pressure Displacement	0.1 MPa	0.15 MPa	0.2 MPa	0.25 MPa	0.3 MPa
-10	21 740.45	22 413.26	23 934.71	25 121.07	25 908.84
-8	21 868.72	22 443.53	23 762.01	25 049.99	26 009.93
-6	21 996.99	22 546.37	23 578.05	24 983.17	26 058.25
-4	22 038.93	22 649.20	23 394.09	24 916.34	26 106.57
-2	22 080.87	22 642.92	23 377.77	24 827.99	26 093.62
0	22 048.19	22 636.65	23 361.45	24 739.63	26 080.67
2	22 015.51	22 684.95	23 409.42	24 623.80	26 076.54
4	22 018.78	22 733.26	23 457.39	24 507.96	26 072.40
6	22 022.05	22 792.23	23 527.75	24 467.97	26 045.27
8	22 094.48	22 851.20	23 598.10	24 427.97	26 018.13
10	22 166.91	22 851.12	23 587.41	24 476.50	25 961.50
Maximum area (mm^2)	426.45	437.94	573.26	693.09	197.74
Maximum relative error	1.40 %	0.99 %	2.45 %	1.54 %	0.66 %

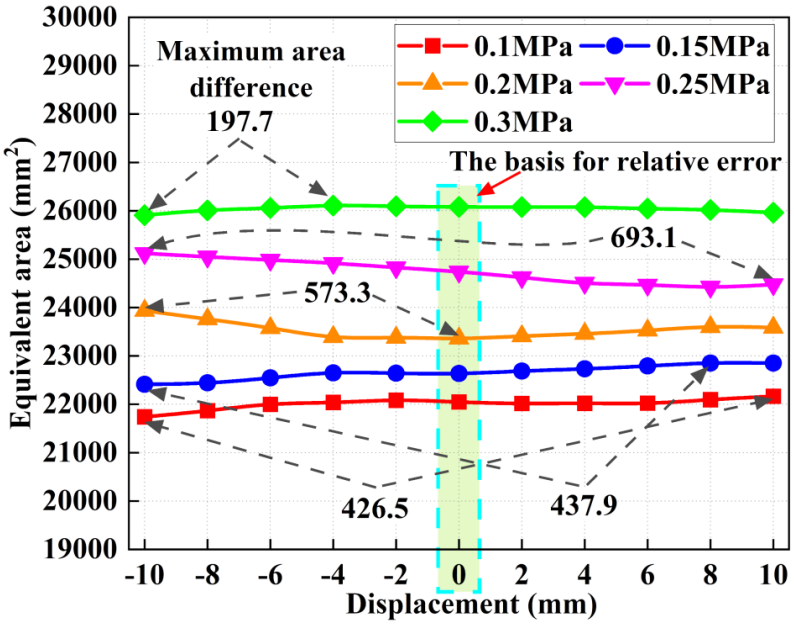

Figure 4. Variation of equivalent effective area within ±10 mm excitation amplitude under different initial internal pressures.

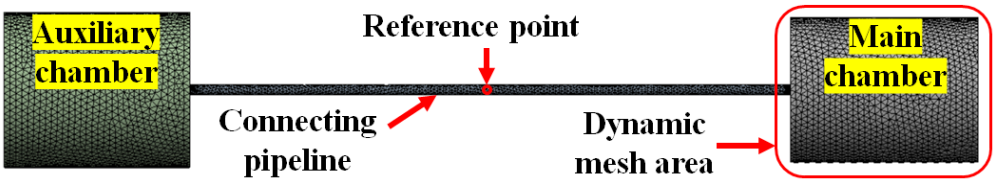

Figure 5. Simplified finite element model of the air spring with auxiliary chamber (ASWAC) internal flow field.

Mesh generation for the computational domain

A conformal algorithm was adopted to ensure the accuracy and efficiency of the simulation (Papkov *et al*., 2023). From the finite element model of the ASWAC, the entire computational domain can be divided into three parts: the main chamber, the auxiliary chamber, and the connecting pipeline. The dimensions of these three parts vary significantly, and the internal gas flow patterns are also different. Therefore, different mesh sizes were selected to discretize each region. Due to the small size of the connecting pipeline and the complexity of its internal flow field, a finer mesh size was required. Thus, preliminary mesh sizes of 1, 2, 3, 4, and 5 mm were selected. The main chamber and the auxiliary chamber have larger dimensions and simpler internal flow fields, allowing for larger mesh sizes. Hence, preliminary mesh sizes of 6, 8, 10, 12, and 14 mm were selected.

Mesh convergence analysis for the computational domain

When the mesh size was reduced to 2 mm, the stiffness was 33.157 N mm^{-1}, requiring approximately 600 min of simulation time (Figure 6). When the mesh size was further reduced to 1mm, the stiffness was 33.139 N mm^{-1}, showing a minimal difference compared to the stiffness at 2 mm, but the simulation time increased to 690 min. Considering both the accuracy and computational efficiency of the simulation, 2 mm was selected as the optimal mesh size for the pipeline. When the piping mesh size was 2 mm, its element quality and skewness were both within acceptable ranges (Table 2). As the mesh size decreased, the stiffness gradually diminished (Figure 7). When the mesh size was reduced to 6 and 8 mm, the stiffness remained stable, and no significant changes were observed, indicating that the influence of mesh size on the simulation results can be neglected at these sizes. The element quality and skewness were both within reasonable ranges when the mesh size was 6 and 8 mm (Table 3). Considering both the accuracy and efficiency of the simulation, the 8 mm mesh size was selected for the chamber.

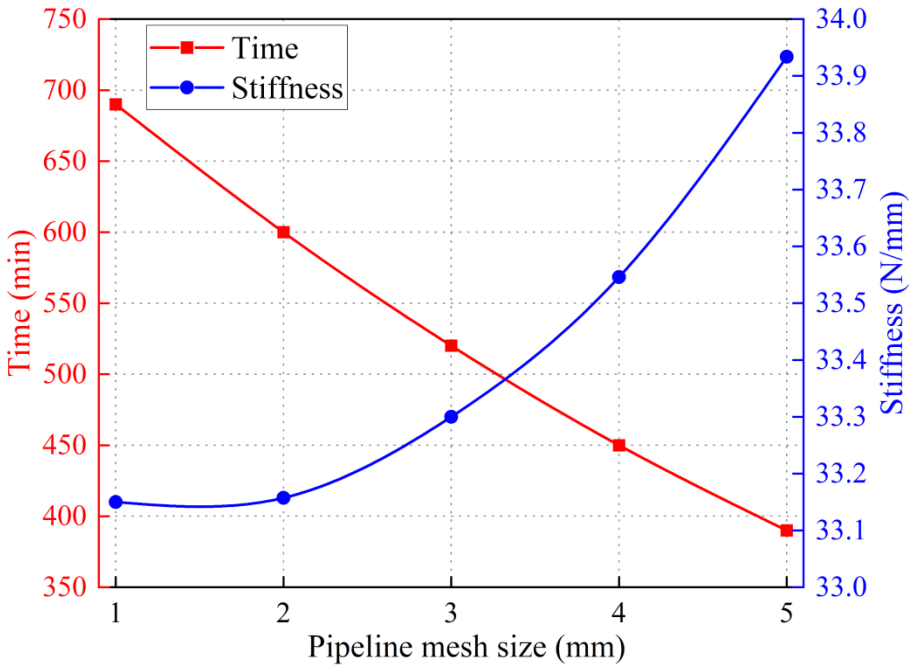

Figure 6. Pipeline mesh independence analysis based on dynamic stiffness and computational time.

Table 2. Element quality and skewness metrics of the pipeline mesh under different mesh sizes.

Mesh size (mm)	1	2	3	4	5
Element quality	0.85082	0.8439	0.84113	0.83949	0.83953
Skewness	0.20701	0.21777	0.22253	0.22565	0.22568

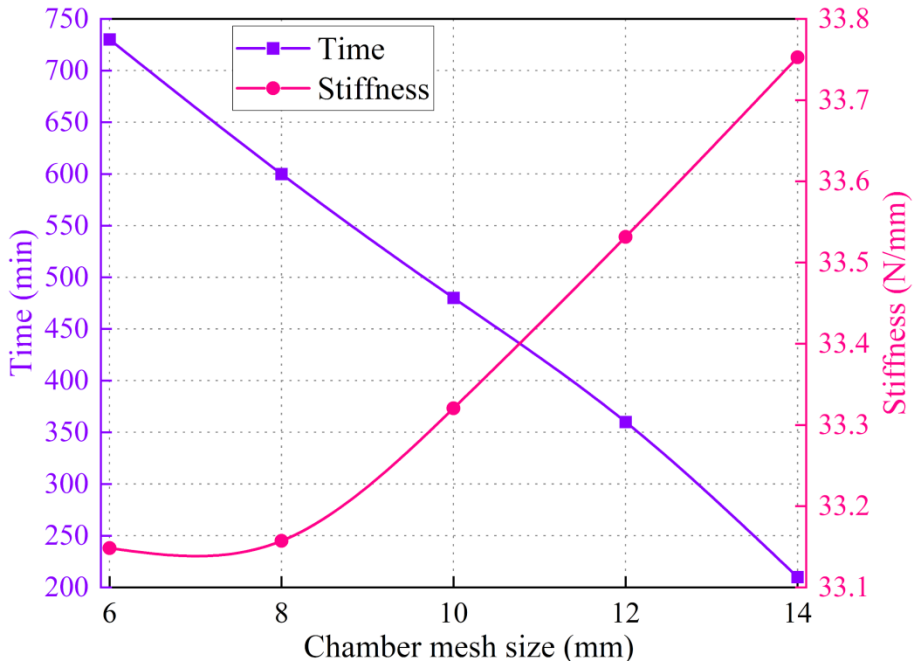

Figure 7. Chamber mesh independence analysis of chamber discretization based on dynamic stiffness response.

Table 3. Element quality and skewness evaluation of the chamber mesh under different mesh sizes.

Mesh size (mm)	6	8	10	12	14
Element quality	0.8438	0.8439	0.8457	0.8464	0.8467
Skewness	0.21808	0.21777	0.21477	0.21363	0.21327

Parameters for the simulation model

Loading pressure

To ensure that the ASWAC had the same load-bearing capacity as the main chamber of the air spring under the same initial internal pressure, the actual internal pressure at the design height of the main chamber of the air spring was considered as the loading pressure for the ASWAC at its design height. The correspondence table details the relationship between the initial internal pressure and the actual internal pressure at the design height (Table 4).

Table 4. Initial internal pressure and actual internal pressure at design height.

Initial internal pressure (MPa)	0.1	0.15	0.2	0.25	0.3
Actual internal pressure (MPa)	0.1497	0.2037	0.2551	0.3066	0.3590

Selection of the auxiliary chamber

Studies have indicated that the air spring performs optimally when the volume ratio of the auxiliary chamber to the main chamber does not exceed two (Constantin *et al*., 2024). The air spring selected for this work has a main chamber volume of approximately 5.4 L. Therefore, the relationship between the volume of the auxiliary chamber and the stiffness of the air spring was explored by selecting auxiliary chamber volumes of 4, 6, 8, and 10 L.

Selection of the connecting pipelines

To minimize the obstruction to air flow caused by the connecting pipeline and to accommodate the installation position of the air spring on the vehicle, a pipeline length of 800 mm was selected for this simulation. Additionally, pipeline diameters of 8, 10, 12, 16, 18, and 20 mm were chosen to investigate their relationship with the stiffness of the air spring.

Extraction of research parameters

After initializing the loading pressure for the ASWAC, a dynamic mesh was utilized to apply a sinusoidal resonant frequency with an amplitude of ±10 mm to the airbag section. The frequency values were the same as those used in the dynamic characteristic analysis of the main chamber, namely 30, 23, 14, 6, and 2 Hz. Concurrently, the surface pressure on the moving part of the airbag mesh surface was recorded when the sinusoidal resonant frequency was applied, and a fitting function was used to obtain the stiffness value of the ASWAC at the design height. Combining different loading frequencies, a total of 250 simulation experiments were conducted, with each simulation lasting approximately 7 h, amounting to a total of 1750 h.

To facilitate further exploration of the relationship between the stiffness of the ASWAC and its internal gas, a reference point inside the connecting pipeline was established. This allowed the measurement of the internal gas flow velocity during the operation of the air spring, with the flow direction from the main chamber to the auxiliary chamber designated as the positive direction. The reference point was positioned in the middle of the connecting pipeline (Figure 5).

RESULTS AND DISCUSSION

Impact of the connecting pipeline diameter (CPD) on the dynamic characteristics of air springs under different initial internal pressure (IIP)

By varying the CPD, the dynamic characteristic curves of the ASWAC at its design height for different CPDs were obtained under various IIPs (Figure 8). The stiffness of CPDs 8 and 10 mm was relatively high at 2 Hz, while the stiffness of CPDs 12, 16, 18, and 20 mm was lower at 2 Hz, with little difference among them. As the loading frequency increased, the stiffness of CPD 8 mm rose rapidly between 2 and 6 Hz but more slowly between 6 and 30 Hz, with the rising speed decreasing as the frequency increased. The stiffness of CPDs 10 and 12 mm increased rapidly between 2 and 14 Hz but more slowly between 14 and 30 Hz, with the rising speed gradually decreasing as the frequency increased. For CPDs 16, 18, and 20 mm, the stiffness increased from slow to fast and then slowed down again between 2 and 30 Hz, with slower increases between 2–6 Hz and 23–30 Hz and faster increases between 6 and 23 Hz.

The stiffness value of CPD 8 mm was the highest at all IIP levels for the respective loading frequencies when comparing 2 and 6 Hz. At 14 Hz, when the IIP was 0.1 and 0.15 MPa, the stiffness value of CPD 8 mm was the highest. However, as the IIP increased to 0.2 and 0.25 MPa, the stiffness values of CPDs 10 and 12 mm surpassed those of 8 mm. At 23 Hz, the stiffness value of CPD 16 mm became the highest. At 30 Hz, the stiffness values increased as CPD decreased.

The flow velocity diagrams at reference points for different CPDs of the ASWAC at its design height (Figure 9) showed that, across different IIPs, the flow velocities of CPDs

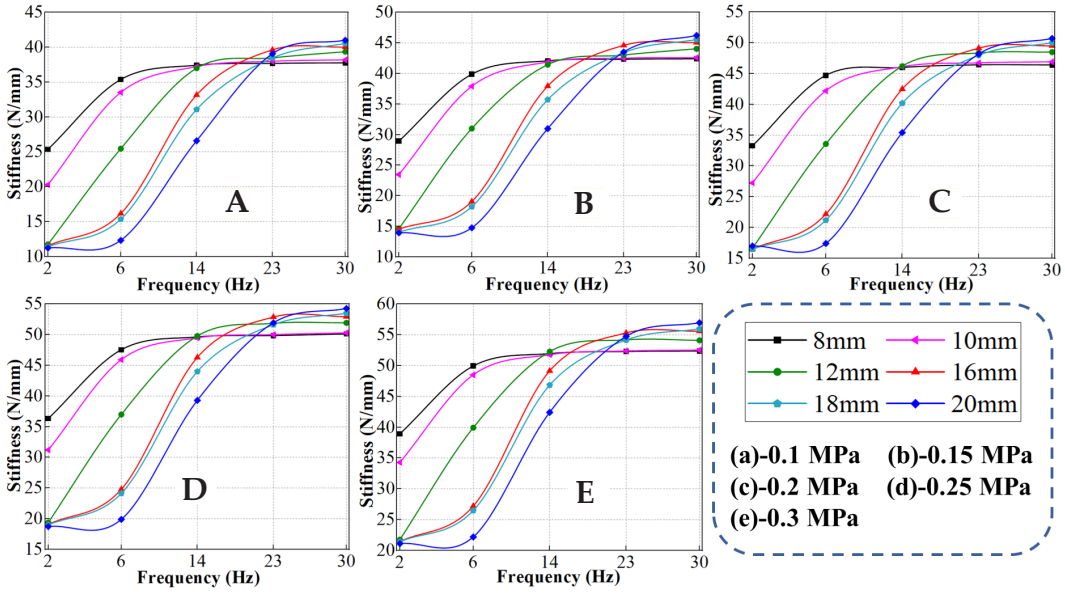

Figure 8. Influence of the connecting pipeline diameter (CPD) under different initial internal pressures (IIP) on the dynamic characteristics of air springs.

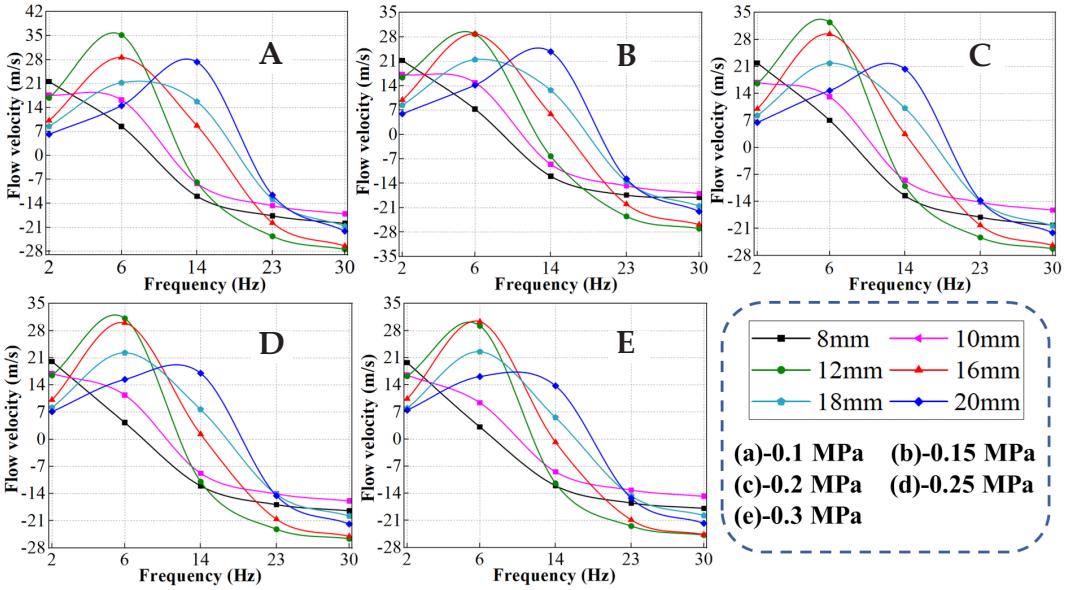

Figure 9. Influence of the connecting pipeline diameter (CPD) on flow velocity inside pipelines under different initial internal pressures (IIP).

8 and 10 mm exhibited a downward trend between 2 and 30 Hz. For CPDs 12, 16, and 18 mm, the flow velocities increased between 2 and 6 Hz and decreased between 6 and 30 Hz. The flow velocity of CPD 20 mm increased between 2 and 14 Hz and decreased between 14 and 30 Hz. At lower loading frequencies, as the frequency increased, the reference point velocity of CPD 8 mm decreased, indicating that internal air choking occurred within CPD 8 mm in this frequency range. As CPD increased, the decrease in reference point velocity shifted to higher frequencies, suggesting that increasing CPD facilitated the additional air chamber's operation at more frequencies. However, excessively increasing the CPD can weaken its damping effect on vibration elimination and increase the difficulty of the vehicle's piping layout.

Under all IIPs, CPDs of 8, 10, and 12 mm exhibited a trend of slow change in both stiffness values and reference point velocity values between the frequencies of 14 and 30 Hz (Figures 8 and 9). Similarly, CPDs of 16, 18, and 20 mm also showed a similar phenomenon between the frequencies of 23 and 30 Hz. It can be concluded that as the loading frequency increases to a certain value, the internal fluid velocity of the CPD will reach a limit value, which determines the maximum stiffness of the air spring.

The influence of the connecting pipeline diameter (CPD) on the dynamic characteristics of air springs at different loading frequencies

The dynamic characteristic curves of ASWAC at the design height for different CPDs were evaluated under various loading frequencies (Figure 10). At a loading frequency of 2 Hz, stiffness increased with increasing IIP. The stiffness of CPD 8 mm was the

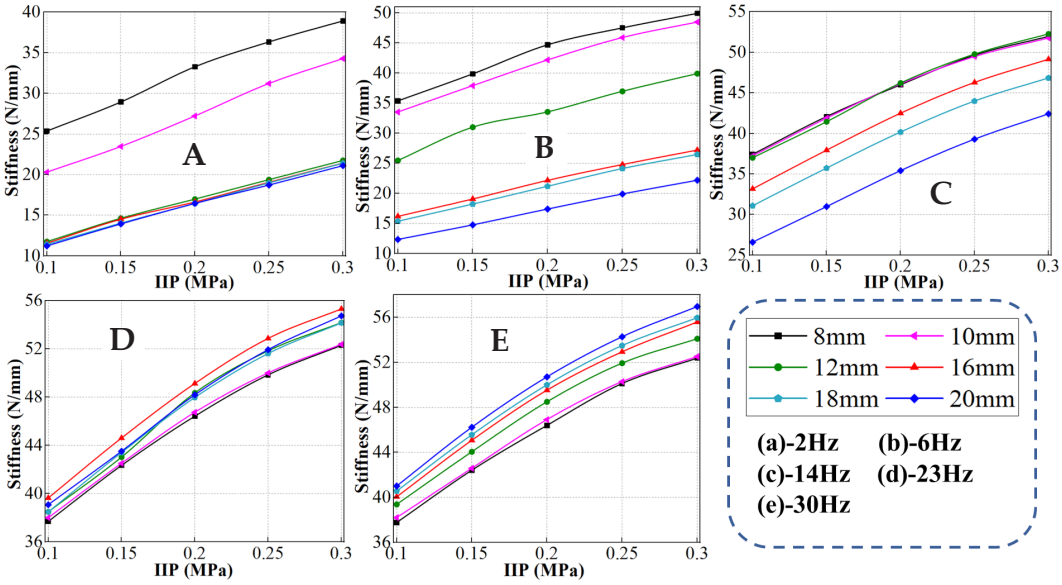

Figure 10. Influence of the connecting pipeline diameter (CPD) on the dynamic characteristics of air springs under different loading frequencies.

highest among all CPDs at all IIPs. At 6 Hz, stiffness exhibited a linear growth trend with increasing IIP. At the same IIP, stiffness decreased as CPD increased. At 14 Hz, stiffness increased with increasing IIP. At the same IIP, the stiffness values of 16, 18, and 20 mm decreased as CPD increased. At 23 Hz, stiffness increased with increasing IIP for all CPDs. At this frequency, the stiffness of 16 mm was the highest among all CPDs at all IIPs. At 30 Hz, stiffness increased with increasing IIP for all CPDs. Compared with 23 Hz, the stiffness values further increased, and the stiffness of 20 mm became the highest among all CPDs at all IIPs. At the same IIP, stiffness increased with increasing CPD.

The overall analysis (Figure 10) revealed that as the loading frequency increased, the stiffness value of CPD 8 mm began to shift, transitioning from being the maximum value at lower IIPs to becoming the minimum value. At a loading frequency of 6 Hz, under the same IIP, the stiffness values of CPD decreased in the order of 8, 10, 12, 16, 18, and 20 mm. However, at a loading frequency of 30 Hz, the stiffness values of CPD increased in the reverse order (20, 18, 16, 12, 10, and 8 mm). This trend was opposite compared to that at a loading frequency of 6 Hz. Overall, under the same IIP, as the loading frequency increased, stiffness decreased while the trend of increasing CPD reversed, establishing a rule that stiffness increases with higher CPD.

The velocity profiles at the reference points for different CPDs at the design height of ASWAC under varying loading frequencies were calculated (Figure 11). At the same IIP, velocity decreased with increasing CPD. In comparison (Figures 10a and 11a), at 2 Hz, CPD 8 mm experienced severe choking, while CPD 10 mm showed mild

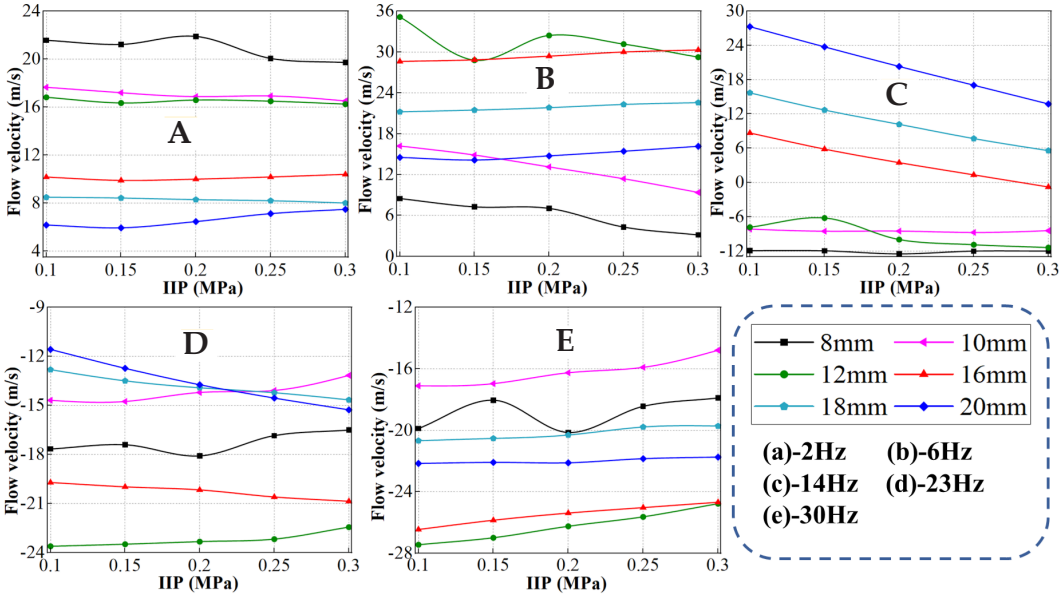

Figure 11. Influence of the connecting pipeline diameter (CPD) on flow velocity inside the pipeline under different loading frequencies.

choking. At 6 Hz, the velocities of CPDs 16, 18, and 20 mm remained stable across different IIPs, whereas CPD 12 mm fluctuated significantly. The velocities of CPD 8 and 10 mm decreased with increasing IIP, and CPD 8 mm reached the lowest positive value. Furthermore, stiffness differences emerged among CPD 12, 16, 18, and 20 mm, indicating that choking occurred in different CPDs as the loading frequency increased (Figures 10b and 11b).

At 14 Hz, the velocities of CPDs 8, 10, and 12 mm first became negative, with CPD 12 mm fluctuating significantly. The velocities of CPDs 16, 18, and 20 mm decreased with increasing IIP, and CPD 16 mm became negative at 0.3 MPa. At the same IIP, the velocities and stiffness values of CPDs 8, 10, and 12 mm were similar, indicating severe choking and reverse flow in these CPDs at 14 Hz (Figures 10c and 11c). The other CPDs showed stiffness differences; however, comparison of the two figures indicated partial choking in their pipelines. At 23 Hz, the velocities of all CPDs became negative, indicating severe choking in all pipelines. The stiffness values of different CPDs were similar across various IIPs, and the regulatory effect of the additional air chamber diminished, corresponding to severe choking at this loading frequency (Figures 10d and 11d).

At 30 Hz, severe choking occurred in all pipelines, with greater reverse flow velocities. The velocities of CPD 8 and 10 mm exceeded those of CPD 20 mm, and CPD 12 mm tended to exceed CPD 16 mm. Smaller CPDs, such as 8 and 10 mm, inhibited the increase in the absolute velocity, resulting in reduced stiffness (Figures 10e and 11e).

Larger CPDs, including 12, 16, 18, and 20 mm, exhibited higher stiffness due to greater absolute velocities. Overall analysis showed that as frequency increased, choking in pipelines of different diameters gradually worsened, particularly in smaller diameters (Figure 11). This indicated that different CPD sizes exerted varying effects on the damping regulation of the additional air chamber. Larger CPDs allowed the additional air chamber to influence stiffness over a wider frequency range.

Influence of auxiliary chamber volume (ACV) on the dynamic characteristics of air springs under different initial internal pressure (IIP)

By adjusting the ACV, the dynamic characteristic curves of ASWAC at the design height were obtained for different ACVs under varying IIPs (Figure 12). For ACVs of 4, 6, and 8 L, stiffness decreased with increasing frequency between 2 and 6 Hz, whereas between 14 and 30 Hz, stiffness increased with frequency. For the 10 L ACV, stiffness increased with frequency across the entire range from 2 to 30 Hz. Across all IIPs, within the frequency range of 2 to 6 Hz, stiffness decreased with increasing ACV at a given frequency. In contrast, between 14 and 30 Hz, stiffness increased with increasing ACV at a given frequency, showing the opposite trend compared to the 2–6 Hz range. This indicated that the influence of ACV on air spring stiffness was largely independent of IIP.

The flow velocity diagrams at the reference point for different ACVs of the ASWAC were obtained at the design height under various IIPs (Figure 13). Across different IIPs, between 2 and 14 Hz, the flow velocity increased with frequency. Between 14

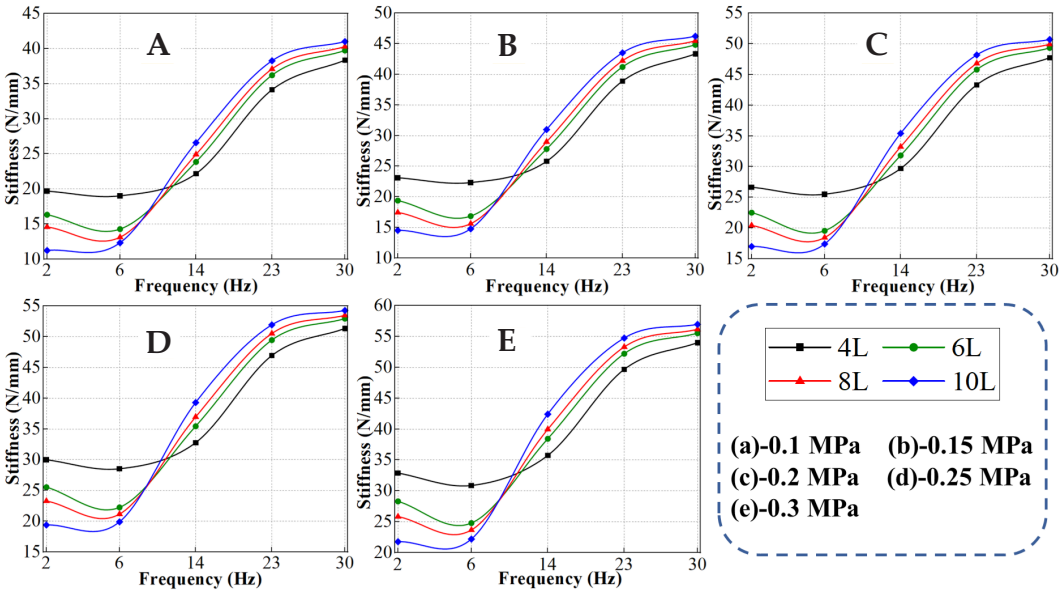

Figure 12. Influence of the auxiliary chamber volume (ACV) under different initial internal pressures (IIP) on the dynamic characteristics of air springs.

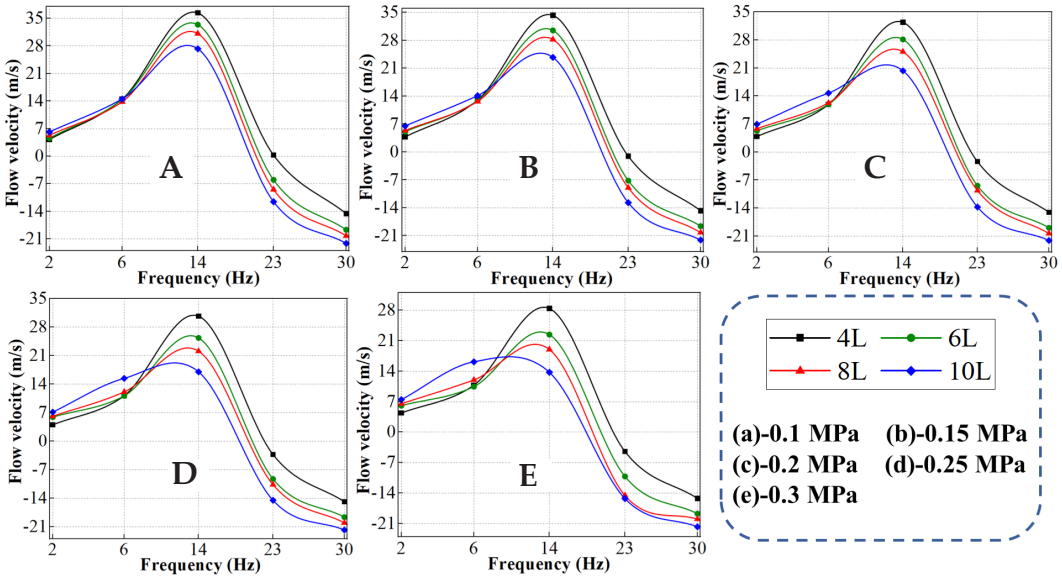

Figure 13. Influence of the auxiliary chamber volume (ACV) on flow velocity inside pipes under different initial internal pressures (IIP).

and 30 Hz, the flow velocity at the reference point decreased with frequency. Under different IIPs, within the frequency range of 14 to 30 Hz, at the same frequency, the flow velocity at the reference point decreased with increasing ACV. Between 14 and 23 Hz, the flow velocity became negative, indicating the occurrence of choking within the pipeline at this point.

Within the frequency ranges of 2–6 and 23–30 Hz, the change in flow velocity at the reference point was relatively slow, corresponding to the slower variation in stiffness within these ranges (Figures 12 and 13). Between 6 and 23 Hz, the flow velocity changed more rapidly, and the stiffness values also varied more significantly within this frequency range.

Influence of the auxiliary chamber volume (ACV) on the dynamic characteristics of air springs under different loading frequencies

The dynamic characteristic curves for different ACVs of the ASWAC at the design height under various loading frequencies were obtained (Figure 14). Across different loading frequencies, stiffness increased with increasing IIP. At higher loading frequencies, the growth rate of stiffness gradually slowed as IIP increased. At loading frequencies of 2 and 6 Hz, stiffness decreased with increasing ACV at the same IIP. However, at loading frequencies of 14, 23, and 30 Hz, stiffness increased with increasing ACV at the same IIP. This finding indicated that as loading frequency increased, the trend shifted from stiffness decreasing with ACV to stiffness increasing with ACV at the same IIP.

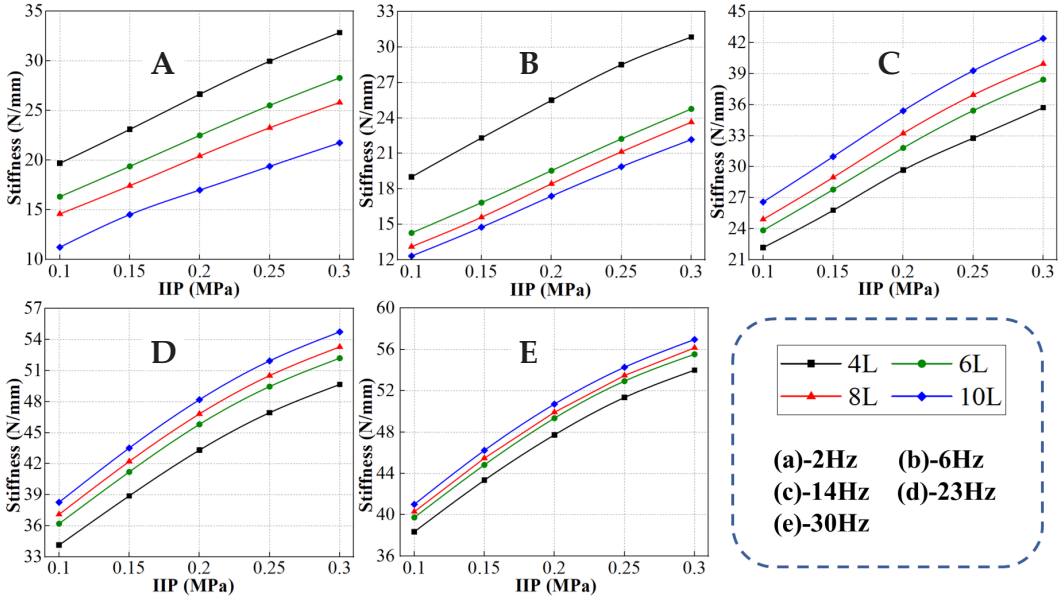

Figure 14. Influence of the auxiliary chamber volume (ACV) on the dynamic characteristics of air springs under different loading frequencies.

The reference point flow velocity diagrams for different ACVs of the ASWAC at the design height under various loading frequencies were obtained (Figure 15). At a loading frequency of 2 Hz and relatively low IIP, choking had already occurred in

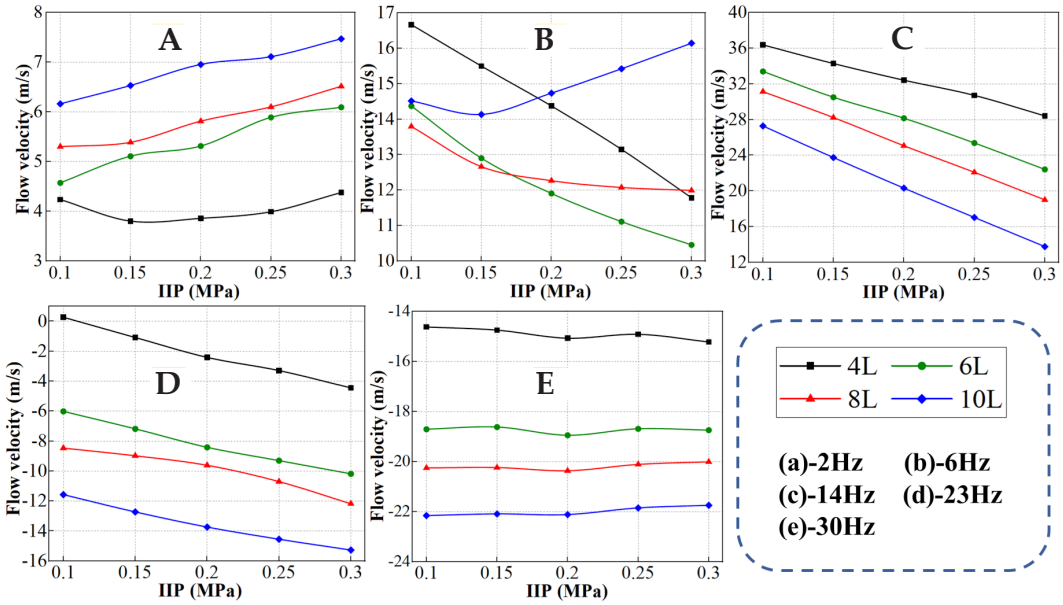

Figure 15. The influence of ACV on flow velocity inside the pipeline under different loading frequencies.

the pipeline of ACV 4 L (Figures 14a and 15a). As IIP increased, the reference point flow velocity continued to increase. At 6 Hz, the flow velocities at the reference point of ACVs 4, 6, and 8 L decreased with increasing IIP, whereas the velocity of ACV 10 L first decreased slightly and then increased with IIP. The decrease in flow velocity at the reference point was most pronounced for ACV 4 L, corresponding to a stiffness value significantly higher than those of the other additional air chambers at this frequency (Figures 14b and 15b).

At 14 Hz, the flow velocities at the reference point of all ACVs decreased with increasing IIP. At the same IIP, the flow velocity decreased with increasing ACV, showing a trend opposite to that observed at 2 Hz. As loading frequency increased to 14 Hz, both stiffness and velocity exhibited trends opposite to those at 2 Hz (Figures 14c and 15c). This indicated that between 2 and 14 Hz, the flow velocity at the reference point reflected the changes in stiffness. At 23 Hz, the flow velocities of all ACVs decreased slightly with increasing IIP. As the variation in flow velocity at the reference point decreased, the differences in stiffness among different ACVs at the same IIP also decreased (Figures 14d and 15d). This result indicated that the influence of ACV on stiffness gradually diminished with increasing IIP. At 30 Hz, the flow velocities at the reference point of all ACVs remained essentially unchanged with variations in IIP. The differences in stiffness among different ACVs at the same IIP became less pronounced (Figures 14e and 15e). At 30 Hz, the influence of ACV on stiffness was minimal.

CONCLUSIONS

Under the same initial internal pressure (IIP), the influence of different connecting pipeline diameters (CPDs) on the dynamic characteristics of the air spring followed the same pattern, with the frequency at which stiffness tended to flatten shifting to higher values as CPD increased. With increasing CPD, the auxiliary chamber influenced stiffness over a wider frequency range. At lower loading frequencies, smaller CPDs exerted a greater influence on stiffness, whereas larger CPDs had a smaller effect. As frequency increased, larger CPDs gradually exerted a stronger influence on stiffness. Between 6 and 30 Hz, at the same IIP, the pattern of stiffness decreasing with diameter gradually shifted to stiffness increasing with diameter.

Under all IIPs, the influence of different auxiliary chamber volumes (ACVs) on the dynamic characteristics of the air spring followed the same pattern. Between 2 and 6 Hz, stiffness decreased with increasing ACV for all IIPs, whereas between 14 and 30 Hz, the opposite trend was observed. At all loading frequencies, particularly at 2 Hz, stiffness decreased with increasing ACV under different IIPs. As loading frequency increased, this trend gradually reversed. Because air springs are subjected to substantial longitudinal loads during operation, this study considered only the influence of longitudinal loads on their static and dynamic characteristics. Future research could investigate and analyze the effects of transverse loads.

ACKNOWLEDGEMENTS

This work was supported by Structural Design and Characteristic Analysis of Automobile Air Spring Shock Absorber (No. H232269).

REFERENCES

Atindana VA, Xu X, Nyedeb AN, Quaisie JK, Nkrumah JK, Assam SP. 2023. The evolution of vehicle pneumatic vibration isolation: A systematic review. Shock and Vibration 2023: 1716615. https://doi.org/10.1155/2023/1716615

Berg M. 2000. A three-dimensional airspring model with friction and orifice damping. Vehicle System Dynamics 33: 528−539. https://doi.org/10.1080/00423114.1999.12063109

Chen C, Hu RR, Huang L. 2011. Study on characteristics of cylindrical air spring. Advanced Materials Research 308–310: 1992–1996. https://doi.org/10.4028/www.scientific.net/amr.308-310.1992

Constantin L, Titurus B, Rendall TCS, de Courcy JJ, Cooper JE. 2024. Experimental analysis of liquid vertical slosh damping at vacuum and atmospheric pressures. Journal of Sound and Vibration 574: 118228. https://doi.org/10.1016/j.jsv.2023.118228

Karachinskii SI, Timofeev OA. 2023. Operation parameters of a gas-dynamic pressure source with explosive initiation. Combustion, Explosion, and Shock Waves 59 (2): 224–228. https://doi.org/10.1134/s0010508223020132

Karpenko M, Stosiak M, Šukevičius Š, Skačkauskas P, Urbanowicz K, Deptuła A. 2023. Hydrodynamic processes in angular fitting connections of a transport machine's hydraulic drive. Machines 11 (3): 355. https://doi.org/10.3390/machines11030355

Kong C, Liu G, Li Y, Yang M, Liao Y, Xia J, Wang Y, Long G. 2025. Multifactor analysis of static and dynamic characteristics of membrane air springs for small passenger cars. Journal of Computational and Nonlinear Dynamics 20 (10): 101005. https://doi.org/10.1115/1.4068976

Kong C, Xia J, Yang M, Li Y, Liao Y. 2024. Analysis of static and dynamic characteristics of membrane air springs for small passenger cars. Journal of the Brazilian Society of Mechanical Sciences and Engineering 46 (12): 682. https://doi.org/10.1007/s40430-024-05244-8

Liu H, Lee JC. 2011. Model development of automotive air spring based on experimental research. *In* 2011 Third International Conference on Measuring Technology and Mechatronics Automation. Institute of Electrical and Electronics Engineers: Shanghai, China. https://doi.org/10.1109/icmtma.2011.433

Mao L, Wei C, Zeng S, Cai M. 2023. Heat transfer mechanism of cold-water pipe in ocean thermal energy conversion system. Energy 269: 126857. https://doi.org/10.1016/j.energy.2023.126857

Mehmood K, Zhang B, Jalal FE, Wan W. 2023. Transient flow analysis for pumping system comprising pressure vessel using unsteady friction model. International Journal of Mechanical Sciences 244: 108093. https://doi.10.1016/j.ijmecsci.2022.108093

Mendia-García I, Gil-Negrete N, Nieto F, Facchinetti A, Bruni S. 2022. Analysis of the axial and transversal stiffness of an air spring suspension of a railway vehicle: mathematical modelling and experiments. International Journal of Rail Transportation 12 (1): 56−75. https://doi.org/10.1080/23248378.2022.2136276

Papkov V, Shadymov N, Pashchenko D. 2023. CFD-modelling of fluid flow in Ansys fluent using python-based code for automation of repeating calculations. International Journal of Modern Physics C 34 (9): 2350114. https://doi.org/10.1142/s0129183123501140

Piller M, Nobile E, Hanratty TJ. 2002. DNS study of turbulent transport at low Prandtl numbers in a channel flow. Journal of Fluid Mechanics 458: 419–441. https://doi.org/10.1017/s0022112001007704Quaglia G, Sorli M. 2001. Air suspension dimensionless analysis and design procedure. Vehicle System Dynamics 35 (6): 443–475. https://doi.org/10.1076/vesd.35.6.443.2040

Toyofuku K, Yamada C, Kagawa T, Fujita T. 1999. Study on dynamic characteristic analysis of air spring with auxiliary chamber. JSAE Review 20 (3): 349–355. https://doi.org/10.1016/s0389-4304(99)00032-6

Van LV, Tung NT. 2023. Application of air suspension system on multi-purpose forest fire fighting vehicle for reducing dynamic load. Journal of Vibration Engineering and Technologies 12 (6): 7219–7230. https://doi.org/10.1007/s42417-023-01069-2

Williams RA. 1997. Automotive active suspensions Part 1: basic principles. Proceedings of the Institution of Mechanical Engineers Part D: Journal of Automobile Engineering 211 (6): 415–426. https://doi.org/10.1243/0954407971526551

Wissink JG. 2003. DNS of separating, low Reynolds number flow in a turbine cascade with incoming wakes. International Journal of Heat and Fluid Flow 24 (4): 626–635. https://doi.org/10.1016/s0142-727x(03)00056-0

Wong P, Deng M, Zhao J, Ghadikolaei MA, Wang H. 2024. Model reference backstepping control for semi-active air suspension systems with parameter uncertainty. Proceedings of the Institution of Mechanical Engineers, Part D: Journal of Automobile Engineering 238 (9): 2650–2659. https://doi.org/10.1177/09544070231173168

Zhang G, Shen G, Can S. 2005. Study on dynamic airspring model with connecting pipe. Journal of the China Railway Society 4: 36–41.

Zhang Z, Wang J, Wu W, Huang C. 2020. Semi-active control of air suspension with auxiliary chamber subject to parameter uncertainties and time-delay. International Journal of Robust and Nonlinear Control 30 (17): 7130–7149. https://doi.org/10.1002/rnc.5169

Zheng E, Fan Y, Zhu R, Zhu Y, Xian J. 2016. Prediction of the vibration characteristics for wheeled tractor with suspended driver seat including air spring and MR damper. Journal of Mechanical Science and Technology 30 (9): 4143–4156. https://doi.org/10.1007/s12206-016-0826-x

Zhu S, Wang J, Zhang Y. 2008. Research on theoretical calculation model for dynamic stiffness of air spring with auxiliary chamber. *In* 2008 IEEE Vehicle Power and Propulsion Conference. Institute of Electrical and Electronics Engineers: Harbin, China. https://doi.org/10.1109/vppc.2008.4677717